Time domain simulation of tandem silicon solar cells with optimal textured light trapping enabled by the quadratic complex rational function

H. Chung,[1] K-Y. Jung,[2] X. T. Tee,[1] and P. Bermel[1,*]

[1]*Birck Nanotechnology Center, Electrical and Computer Engineering, 1205 W. State St, West Lafayette, Indiana*
[2] *Department of Electronic Engineering, Hanyang University, Seoul, South Korea*
∗pbermel@purdue.edu

Abstract: Amorphous silicon/crystalline silicon (a-Si/c-Si) micromorph tandem cells, with best confirmed efficiency of 12.3%, have yet to fully approach their theoretical performance limits. In this work, we consider a strategy for improving the light trapping and charge collection of a-Si/c-Si micromorph tandem cells using random texturing with adjustable short-range correlations and long-range periodicity. In order to consider the full-spectrum absorption of a-Si and c-Si, a novel dispersion model known as a quadratic complex rational function (QCRF) is applied to photovoltaic materials (e.g., a-Si, c-Si and silver). It has the advantage of accurately modeling experimental semiconductor dielectric values over the entire relevant solar bandwidth from 300—1000 nm in a single simulation. This wide-band dispersion model is then used to model a silicon tandem cell stack (ITO/a-Si:H/c-Si:H/silver), as two parameters are varied: maximum texturing height h and correlation parameter f. Even without any other light trapping methods, our front texturing method demonstrates 12.37% stabilized cell efficiency and 12.79 mA/cm^2 in a 2 μm-thick active layer.

References and links

1. R. Margolis, Ed. *SunShot vision study* (U.S. Department of Energy, 2012).
2. N.S. Lewis, "Toward Cost-Effective Solar Energy Use," Science **315**, 798-801 (2007).
3. P. Bermel, C. Luo, L. Zeng, L. C. Kimerling, and J. D. Joannopoulos, "Improving thin-film crystalline silicon solar cell efficiencies with photonic crystals," Optics Express **15**, 16986–17000 (2007).
4. A. G. Aberle, "Thin-film solar cells," Thin Solid Films **517**, 4706–4710 (2009).
5. J. G. Mutitu, S. Shi, C. Chen, T. Creazzo, A. Barnett, C. Honsberg, and D. W. Prather, "Thin film solar cell design based on photonic crystal and diffractive grating structures," Optics Express **16**, 15238–15248 (2008).
6. M.A. Green, K. Emery, Y. Hishikawa, W. Warta and E.D. Dunlop, "Solar cell efficiency tables (version 43)," Prog. Photovolt.: Res. Appl. **21**, 1–9 (2013).
7. W. Shockley and H. J. Queisser, "Detailed balance limit of efficiency of p-n junction solar cells," Journal of applied physics **32**, 510–519 (1961).
8. A. De Vos, "Detailed balance limit of the efficiency of tandem solar cells," J. Phys. D **13**, 839846 (1980).
9. O. D. Miller, E. Yablonovitch, and S. R. Kurtz, "Strong internal and external luminescence as solar cells approach the shockley-queisser limit," IEEE J. Photovolt. **2**, 303311 (2012).

10. M. Berginski, J. Hupkes, M. Schulte, G. Schope, H. Stiebig, B. Rech, and M. Wuttig, "The effect of front zno: Al surface texture and optical transparency on efficient light trapping in silicon thin-film solar cells," Journal of Applied Physics **101**, 074903–074903 (2007).

11. R. Brendel, M. Hirsch, R. Plieninger, and J. Werner, "Quantum efficiency analysis of thin-layer silicon solar cells with back surface fields and optical confinement," IEEE Transactions on Electron Devices **43**, 1104–1113 (1996).

12. T. Tiedje, E. Yablonovitch, G. D. Cody, and B. G. Brooks, "Limiting efficiency of silicon solar cells," IEEE Transactions on Electron Devices **31**, 711–716 (1984).

13. E. Yablonovitch, "Statistical ray optics," JOSA **72**, 899–907 (1982).

14. M. Ghebrebrhan, P. Bermel, Y. Avniel, J. D. Joannopoulos, and S. G. Johnson, "Global optimization of silicon photovoltaic cell front coatings," Optics express **17**, 7505–7518 (2009).

15. J. Zhao, A. Wang, M. A. Green, and F. Ferrazza, "19.8% efficient honeycomb textured multicrystalline and 24.4% monocrystalline silicon solar cells," Applied Physics Letters **73**, 1991 (1998).

16. R. Dewan, I. Vasilev, V. Jovanov, and D. Knipp, "Optical enhancement and losses of pyramid textured thin-film silicon solar cells," Journal of Applied Physics **110**, 013101 (2011).

17. C. L. Tan, A. Karar, K. Alameh, and Y. T. Lee, "Optical absorption enhancement of hybrid-plasmonic-based metal-semiconductor-metal photodetector incorporating metal nanogratings and embedded metal nanoparticles," Optics express **21**, 1713–1725 (2013).

18. C. Rockstuhl, S. Fahr, K. Bittkau, T. Beckers, R. Carius, F.-J. Haug, T. Söderström, C. Ballif, and F. Lederer, "Comparison and optimization of randomly textured surfaces in thin-film solar cells," Optics express **18**, A335–A341 (2010).

19. S.-S. Lo, C.-C. Chen, F. Garwe, and T. Pertch, "Broad-band anti-reflection coupler for a: Si thin-film solar cell," Journal of Physics D: Applied Physics **40**, 754 (2007).

20. J. Lacombe, O. Sergeev, K. Chakanga, K. von Maydell, and C. Agert, "Three dimensional optical modeling of amorphous silicon thin film solar cells using the finite-difference time-domain method including real randomly surface topographies," Journal of Applied Physics **110**, 023102 (2011).

21. Y.-C. Tsao, C. Fisker, and T. Garm Pedersen, "Optical absorption of amorphous silicon on anodized aluminum substrates for solar cell applications," Optics Communications **315**, 17–25 (2014).

22. V. Jovanov, U. Palanchoke, P. Magnus, H. Stiebig, J. Hüpkes, P. Sichanugrist, M. Konagai, S. Wiesendanger, C. Rockstuhl, and D. Knipp, "Light trapping in periodically textured amorphous silicon thin film solar cells using realistic interface morphologies," Optics Express **21**, A595–A606 (2013).

23. A. Tavlove and S. C. Hagness, "Computational electrodynamics: the finite-difference time-domain method," Second Edition, Artech House, (Artech House, 2000).

24. W. C. Chew, *Waves and fields in inhomogenous media* (Van Nostrand Reinhold, 1990).

25. G. Jellison and F. Modine, "Parameterization of the optical functions of amorphous materials in the interband region," Applied Physics Letters **69**, 371–373 (1996).

26. A. Fantoni and P. Pinho, "FDTD simulation of light propagation inside a-si: H structures," in "MRS Proceedings," (Cambridge University, 2010), vol. 1245, 1245–A15.

27. S.-G. Ha, J. Cho, J. Choi, H. Kim, and K.-Y. Jung, "FDTD dispersive modeling of human tissues based on quadratic complex rational function," IEEE Transactions on Antennas and Propagation **61**, 996–999 (2013).

28. H. Chung, J. Cho, S.-G. Ha, S. Ju, and K.-Y. Jung, "Accurate FDTD dispersive modeling for concrete materials." ETRI Journal **35**, 915–918, (2013).

29. H. Chung, S.-G. Ha, J. Cho, and K.-Y. Jung, "Accurate FDTD modeling for dispersive media using rational function and particle swarm optimization." International Journal of Electronics **to be published** (2014).

30. K. Yamamoto, A. Nakajima, M. Yoshimi, T. Sawada, S. Fukuda, T. Suezaki, M. Ichikawa, Y. Koi, M. Goto, H. Takata, T. Sasaki, and Y. Tawada, "Novel hybrid thin film silicon solar cell and module," *in Proceedings of 3rd World Conference on Photovoltaic Energy Conversion* (IEEE, 2003), vol. 3, pp. 2789–2792.

31. F. L. Teixeira, "Time-domain finite-difference and finite-element methods for maxwell equations in complex media," IEEE Transactions on Antennas and Propagation **56**, 2150–2166 (2008).

32. C. Herzinger, B. Johs, W. McGahan, J. Woollam, and W. Paulson, "Ellipsometric determination of optical constants for silicon and thermally grown silicon dioxide via a multi-sample, multi-wavelength, multi-angle investigation," Journal of Applied Physics **83**, 3323–3336 (1998).

33. A. F. Oskooi, D. Roundy, M. Ibanescu, P. Bermel, J. D. Joannopoulos, and S. G. Johnson, "Meep: A flexible free-software package for electromagnetic simulations by the fdtd method," Computer Physics Communications **181**, 687–702 (2010).

34. E. L. Haines and A. B. Whitehead, "Pulse height defect and energy dispersion in semiconductor detectors," Review of Scientific Instruments **37**, 190–194 (1966).

35. R. Collins, A. Ferlauto, G. Ferreira, C. Chen, J. Koh, R. Koval, Y. Lee, J. Pearce, and C. Wronski, "Evolution of microstructure and phase in amorphous, protocrystalline, and microcrystalline silicon studied by real time spectroscopic ellipsometry," Solar Energy Materials and Solar Cells **78**, 143–180 (2003).

36. E. D. Palik, *Handbook of Optical Constants of Solids* (Academic Press, 1998).

37. S. J. Orfanidis, *Electromagnetic waves and antennas* (Rutgers University, 2002).

38. L. T. Varghese, Y. Xuan, B. Niu, L. Fan, P. Bermel, and M. Qi, "Enhanced photon management of thin-film silicon solar cells using inverse opal photonic crystals with 3d photonic bandgaps," Advanced Optical Materials **1**, 692–698 (2013).

39. S. Wiesendanger, M. Zilk, T. Pertsch, F. Lederer, and C. Rockstuhl, "A path to implement optimized randomly textured surfaces for solar cells," Applied Physics Letters **103**, 131115 (2013).

40. M. J. Keevers, T. L. Young, U. Schubert, and M. A. Green, "10% efficient CSG minimodules," Proceedings of the 22nd European Photovoltaic Solar Energy Conference and Exhibition, Milan (2007).

41. Z. Yu, A. Raman, and S. Fan, "Nanophotonic light-trapping theory for solar cells," Applied Physics A **105**, 329–339 (2011).

42. Z. Yu, A. Raman, and S. Fan, "Thermodynamic upper bound on broadband light coupling with photonic structures," Physical review letters **109**, 173901 (2012).

43. J. L. Gray, X. Wang, X. Sun, and J. R. Wilcox, "Adept 2.0," (2011).

44. A. Bielawny, J. Üpping, P. T. Miclea, R. B. Wehrspohn, C. Rockstuhl, F. Lederer, M. Peters, L. Steidl, R. Zentel, S.-M. Lee, M. Knez, A. Lambertz, and R. Carius, "3d photonic crystal intermediate reflector for micromorph thin-film tandem solar cell," physica status solidi (a) **205**, 2796–2810 (2008).

45. J. Üpping, A. Bielawny, R. B. Wehrspohn, T. Beckers, R. Carius, U. Rau, S. Fahr, C. Rockstuhl, F. Lederer, M. Kroll, T. Pertsch, L. Steidl, and R. Zentel, "Three-dimensional photonic crystal intermediate reflectors for enhanced light-trapping in tandem solar cells," Advanced Materials **23**, 3896–3900 (2011).

46. D. Madzharov, R. Dewan, and D. Knipp, "Influence of front and back grating on light trapping in microcrystalline thin-film silicon solar cells," Optics express **19**, A95–A107 (2011).

47. H. Sai, H. Fujiwara, M. Kondo, and Y. Kanamori, "Enhancement of light trapping in thin-film hydrogenated microcrystalline si solar cells using back reflectors with self-ordered dimple pattern," Applied Physics Letters **93**, 143501–143501 (2008).

48. K. Yamamoto, A. Nakajima, M. Yoshimi, T. Sawada, S. Fukuda, T. Suezaki, M. Ichikawa, Y. Koi, M. Goto, T. Meguro, T. Matsuda, M. Kondo, T. Sasaki, and Y. Tawada, "A high efficiency thin film silicon solar cell and module," Solar Energy **77**, 939–949 (2004).

1. Introduction

Sunlight is one of the most promising renewable sources of energy. The amount of solar power incident on the Earth's surface is 10,000 times greater than the commercial energy used by every human on the planet, even without assuming any improvements in the performance and cost of current solar cell technology [1]. In recent years, the level of adoption of solar technology has increased enormously, to tens of gigawatts of annual installations worldwide. However, the enormous potential of this resource may not be realized without further improvements in the efficiency of materials usage, and greater reductions in cost of manufacturing, particularly for incumbent technologies based on silicon [2]. For example, the fluctuating prices of polysilicon wafers have provided significant motivation for the development and utilization of thin film solar cells (TFSCs). TFSCs have a major advantage over ordinary, wafer-based solar cell technology, i.e., they provide the same power with only a fraction of the materials usage [3–5]. However, the maximum efficiencies of some types of TFSCs are lower than those found in wafer-based technology. For example, the best crystalline silicon-based solar cells operate at 25.0% efficiency, whereas nanocrystalline silicon TFSCs only have efficiencies up to 10.7% [6].

The gap in performance between TFSCs and monocrystalline-based cells is believed to arise primarily from differences in optical and electronic design and performance. Because of incomplete light absorption, many photovoltaic cells have lower performance than the theoretical Shockley-Queisser limit associated with their electronic bandgap [7]. This is particularly a challenge for thin-film materials with low mobilities. Among the variety of commercially manufactured photovoltaic materials, silicon micromorph solar cells have operated far from the theoretical limit of tandem cells: approximately 40% with a-Si (Eg_1 = 1.72eV) and c-Si (Eg_2 = 1.11eV) [8, 9]. On the other hand, thin film silicon micromorph cells have a record efficiency of only 12.3% [6]. Thus, it is very important to identify the best light-trapping structures possible to help maximize the performance and reduce the costs of photovoltaic cells. Light trapping can be achieved by changing the angle of the light as it travels in the solar cell, i.e., by elongating the optical path, and this can be done by using a surface that has a rough texture. Theoreti-

cally, a rough-textured surface reduces reflection by increasing the probability that the reflected light will bounce back onto the surface, minimizing its chance of reflecting out of the cell [10]. From early theoretical work on photovoltaic cells [11, 12], it is known that a perfectly random structure can scatter light at all possible angles inside the active layer, thereby enhancing the absorption (effective path length) up to $4n^2$ [13]. However, thin-film solar cells, in particular, rarely achieve such high performance [14]. Part of the reason is that analytical approaches do not adequately describe the real structures that have been built experimentally. In particular, the feature size of a randomly-textured surface seems to play an important role for light absorption, based on experimental observations over the last decade [15, 16]. Although experimental results must be the ultimate guide, examining and optimizing a very wide range of structures that can potentially be fabricated is extremely expensive and time-consuming. Thus an extremely accurate, simulation-based approach is needed to help guide experimentalists. In this work, we investigate and optimize a broad class of random structures with short-range correlation for experimental realism, and long range periodicity to enhance diffraction into guided modes. As depicted in Fig. 1, the simulation of random texturing is not a trivial undertaking due to the complicated structure and dispersion characteristics of a thin film solar cells.

Most previous simulation works related to TFSC materials, especially the case of an a-Si solar cell, have been conducted in the frequency domain, either with just a single frequency at a time [17–20], a limited range of frequencies [21], or split frequencies [22]. For a single frequency simulation, it should be emphasized that runtime increases linearly with the number of frequencies, and thus a single frequency method is not suitable in the presence of sharp spectral features, such as those engendered by a 3D dispersive material. As an alternative, the finite difference time domain (FDTD) method sidesteps this problem by simulating all frequencies at once in a single simulation, which can finish quickly in the presence of loss [23, 24]. However, most thin film photovoltaic materials do not have a proper time domain dispersion model, because semiconductor materials generally do not follow the Drude-Lorentz model over the whole range of wavelengths due to multiple optical transitions and varying joint densities of states [25]. The dispersion characteristics of thin film photovoltaic materials have been investigated extensively over a long period of time. Among many dispersion models, the Tauc-Lorentz (TL) model captures the characteristics of a-Si material very well, including varying joint densities of states for optical transitions [25]. However, the TL model is not sufficient for time domain simulations due to the complexity of its equation, which makes the resulting FDTD implementation computationally expensive. Thus the Double-Lorentz (DL) model was suggested as an alternative for the time domain simulation of a-Si material [26]. However, since the DL model must have a negative pole in its dispersion equation, the stability of 2-D and 3-D simulations cannot be guaranteed when the DL model is used.

In this work, we apply a quadratic complex rational function (QCRF) model to accurately capture the dispersion of thin film photovoltaic materials. We employ a FDTD simulation due to its simplicity and accuracy [27–29]. Specifically, the dielectric function of a-Si is modeled over the wavelength range from 300—1000 nm, where the relevant power-generating absorption of the a-Si active layer mainly occurs. A full-wave optical simulation is performed and the full-spectrum results are compared to an analytic model as well as experimental data. Also, it has been shown that the QCRF model can fit other photovoltaic materials including, but not limited to, c-Si, silver, and CdTe.

In order to trap light optimally, we suggest a statistically correlated random surface texturing algorithm which can reproduce known structures such as perfectly Lambertian surfaces and flat surfaces in the proper limits, as well as yielding physically realistic structures at intermediate values. Combining this proposed texturing with accurate modeling of TFSC materials can then be used to determine the optimum texturing of the front surface texturing of a tandem silicon
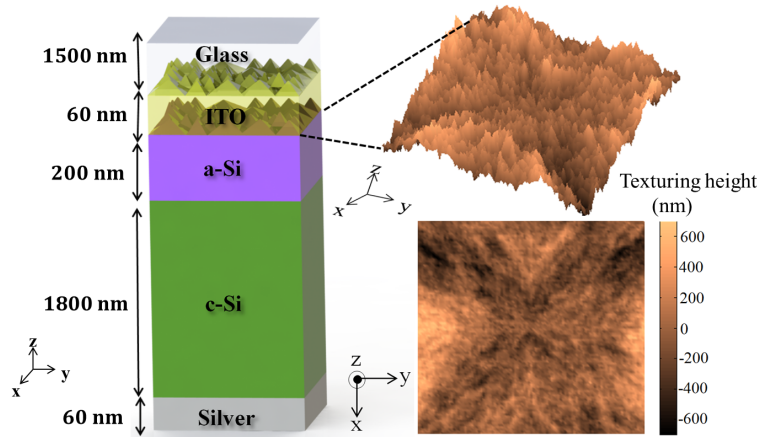
Fig. 1. Cross section of a-Si/c-Si tandem solar cell. It is contacted with indium tin oxide on the front, and silver in the back, and encapsulated with glass. The randomly textured front surface is shown from two different perspectives. Note that the same textured surface on the ITO and a-Si is also applied to the top of the c-Si layer. The minimum glass thickness of 1500 nm is used only in simulation. Experimental thicknesses are greater, but Fig. 4 shows that this only has a minor effect on the absorption spectrum.

solar cell (a-Si/c-Si) structure with normal incident light, as shown in Fig. 1. The tandem silicon solar cell has several advantages over a silicon-based single junction solar cell [30]. For instance, the tandem silicon cell is more stable than the a-Si:H single junction solar cell, due to the contribution of a bottom μc-Si:H cell, which means that the Staebler-Wronski degradation is smaller. In contrast with the single μc-Si:H single junction solar cell, it can be manufactured as a thinner layer. However, one additional challenge is that unlike a single junction solar cell, a multi-junction solar cell must have the currents generated in each layer matched in order to obtain optimal performance. This requirement further suggests that careful simulation will be necessary for a successful design.

2. Dispersion modeling and validation of its accuracy

Classical modeling methods, such as the Debye, Lorentz and Drude models, have been used extensively for many types of dispersive media [23, 31–33]. However, those models are insufficient for dispersive modeling of some thin film photovoltaic materials such as a-Si, CIGS and CZTS, because in the semiconductor materials, both the conducting term and non-conducting term must be taken into account in their wave equation. The wave equation considering both terms is rather complicated and the solutions are somewhat difficult to interpret [34]. Nevertheless, a qualitative description of many of the optical properties of semiconductors is furnished by classical theory. As a result, there is a promising modeling method called Tauc-Lorentz model [25] which shows very good agreement with measurements of a-Si. However, the Tauc-Lorentz model has an exponential function in its equation, making numerical differentiation very difficult; thus, the Tauc-Lorentz model is not ideal for time domain simulations [26]. Recently, the quadratic complex rational function (QCRF) model was suggested for dispersive modeling of biological tissues [27] and concrete materials [28], although its potentially usefulness is much more general. The QCRF dielectric function has the following form:

$$\varepsilon_{r,QCRF}(\omega) = \frac{A_0 + A_1(j\omega) + A_2(j\omega)^2}{1 + B_1(j\omega) + B_2(j\omega)^2}, \tag{1}$$

where ω is the optical frequency, and A_0, A_1, A_2, B_1, and B_2 are adjustable parameters.

As shown in Eq. (1), the QCRF dispersion model has an advantage over the Drude, Debye and Lorentz dispersion models in terms of the number of degrees of freedom, which helps make it highly applicable to wide-band dispersive media such as photovoltaic materials. In addition, the coefficients of the QCRF model can be obtained by solving a 5×5 matrix inversion analytically — a very computationally efficient procedure [27–29]. In this paper, the QCRF model is applied to thin film photovoltaic materials.

2.1. Dispersion modeling

Despite the simplicity and accuracy of the QCRF method, the conventional QCRF model does not always precisely fit measurements of all materials, especially when the imaginary part of epsilon exponentially approaches zero. Also, obtaining the coefficients of the QCRF model through matrix inversion does not consider the Kramers-Kronig (K-K) relations explicitly. However, an optimization method respecting K-K can be used to overcome this limitation [29].

As shown in Fig. 2, the QCRF model fits fairly well with measurement data for photovoltaic materials. Since the light absorbed by a dispersive material is directly proportional to an exponential of ε'', the imaginary part of the dielectric function of a-Si, the imaginary part of the dielectric function of which varies sharply, is plotted as a log scale. Also, in this work, silver is treated as a non-absorbing material, so only the real part of permittivity is considered. Although it is possible to fit lossy silver with the QCRF model, if we were to treat silver as a lossy material explicitly, it would result in a predictive error, in which parasitic loss would be incorrectly counted as absorption contribution to open-circuit voltage. This means that our estimates of short-circuit current enhancement may slightly underestimate the relative enhancement associated with our light-trapping approach. The optical constants of the photovoltaic materials considered in this manuscript were acquired from the literature [35, 36].

2.2. Theoretical absorption and simulation result

In this section, the accuracy of the QCRF model is verified by comparison to analytical predictions for a dielectric slab. In the 300 nm thickness of a single a-Si dielectric slab, the 3-D FDTD simulation results are compared to analytic absorption derived by a theoretical calculation [37]. The total reflection and transmission coefficients for the electric fields can be calculated analytically using multiple reflections, and then summed exactly to yield:

$$r(\lambda) = \rho_1 + \sum_{n=1}^{\infty} \tau_1 \tau_1' (\rho_1')^{n-1} \rho_2^n e^{-j\omega t} = \rho_1 + \frac{\tau_1 \tau_1'}{\rho_2^{-1} e^{j\omega t} - \rho_1'} \tag{2}$$

$$t(\lambda) = \tau_1 \tau_2 \sum_{n=0}^{\infty} \left(\rho_2 \rho_1' \right)^n e^{-j\omega t} = \frac{\tau_1 \tau_2}{1 - \rho_2 \rho_1' e^{-j\omega t}}, \tag{3}$$

where ρ_1 is the electric field reflection coefficient at the left boundary of the dielectric slab when traveling to the right, ρ_1' is the same coefficient when traveling in the reverse direction, τ_1 is the transmission at the left boundary when traveling to the right, τ_1' is the same coefficient traveling in the reverse direction, ρ_2 is the reflection coefficient at the right boundary of the dielectric slab when traveling to the right, $\omega = 2\pi c/\lambda$ is the optical frequency, and t is time required for light travel through the certain thickness of dielectric material. Note that $\tau_k = 1 + \rho_k$ and $\tau_k' = 1 + \rho_k'$
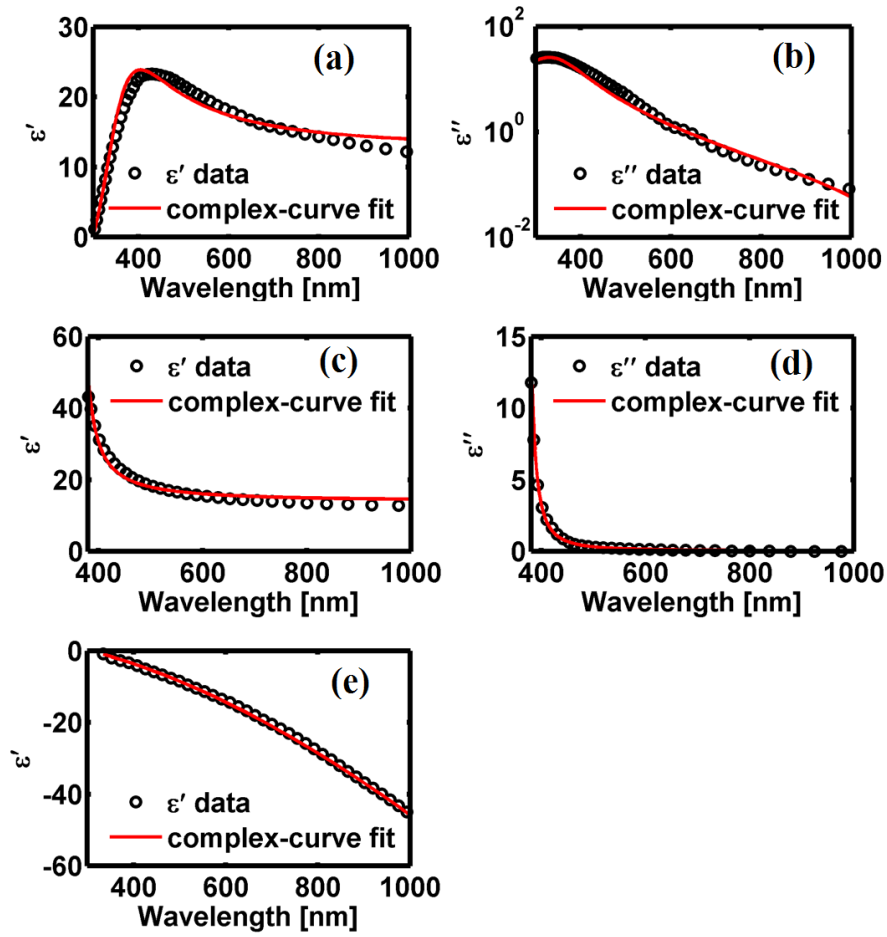
Fig. 2. Dispersion curve fittings of photovoltaic materials using the QCRF model. The solid lines and symbols indicates the results of the QCRF model and the experimental data of dispersive material, respectively: (a) Real part of relative permittivity of a-Si. (b) Imaginary part of relative permittivity of a-Si. (c) Real part of relative permittivity of c-Si. (d) Imaginary part of relative permittivity of c-Si. (e) Real part of relative permittivity of silver.
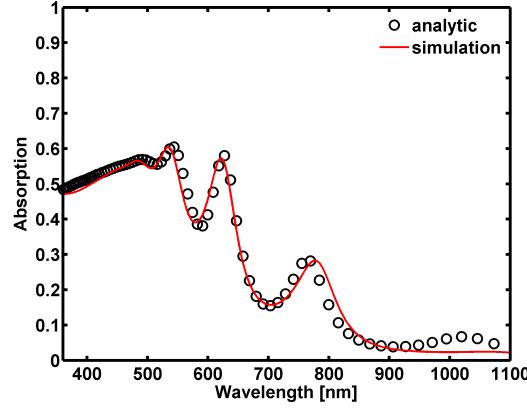
Fig. 3. The theoretical and simulated absorption rates of 300 nm thick a-Si, the former being obtained from Eq. (3) combined with literature data from ref. [36], and the latter being obtained from our QCRF model. The root mean square error from comparing the two data sets is 3.97%.

for all integer k, because of phase shifts. Using Eqs. (2) and (3), reflected power $R(\lambda) = |r(\lambda)|^2$ and transmitted power $T(\lambda) = |t(\lambda)|^2$ can also be obtained. The light absorption spectrum $A(\lambda)$ is then given simply by $A(\lambda) = 1 - T(\lambda) - R(\lambda)$.

Using this approach, the light absorption spectrum for a 300 nm dielectric slab of a-Si is obtained. Also, a 3-D QCRF based FDTD simulation is performed with 300 nm thickness of a-Si material. The dispersive QCRF material is located at the center of 3-D space which has 100 $\times$ 100 $\times$ 900 cells. The x and y boundaries are connected periodically; perfectly matched layers are implemented near the z boundaries (at the top and bottom of the simulation geometry). The Yee lattice spacing is set to 3.86 nm, resulting in the minimum resolution of 20 cells per optical wavelength within all non-metallic materials. The rest of the simulation region is set to be free space.

As shown in Fig. 3, the dispersive FDTD simulation, which is performed only once, predicts the absorption of the a-Si material very accurately, including both the material dispersion and the Fabry-Perot oscillations that occur in the dielectric slab. Comparing the two data sets, we find that the root mean square error between them is 3.97%.

2.3. Experimental and simulated absorption result in the solar cell structure

This section presents the results of the 3-D FDTD simulation of a c-Si single junction solar cell structure found in a recent experiment. In this experimental study, the absorption of the solar cell was measured over a broad range of wavelengths both with and without light trapping. The thickness of c-Si layer is 1500 nm and ITO is considered as a charge transport and anti-reflection coating layer [38]. A 3-D QCRF-FDTD simulation is performed on the same geometries in order to establish its accuracy.

The experimentally measured absorption spectra of c-Si solar cells, shown on the left hand side of Fig. 4, can be predicted accurately using our simulation technique. More specifically, the absorption spectrum measured for the flat structure is very similar to our simulation results, except for the Fabry-Perot oscillations in the short wavelength range. This difference is mainly because the experiment had glass that is more than 100 μm thick deposited on the top of the solar cell, whereas, in order to save simulation time, it is assumed that the thickness of the glass is less than a few microns. Even so, the overall absorption curve for the flat case matches
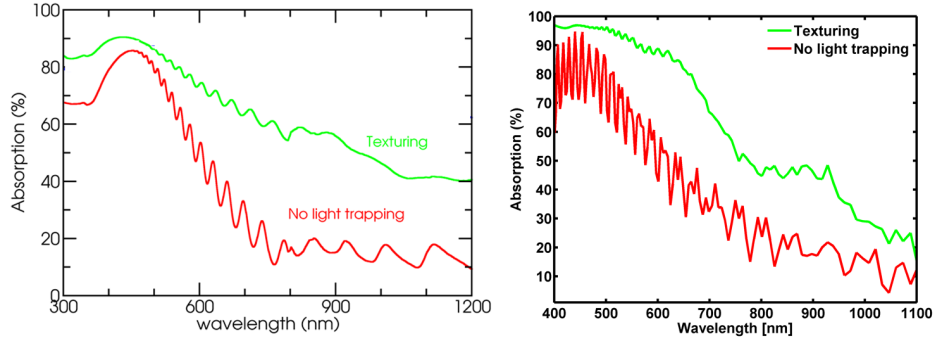
Fig. 4. The left figure indicates the experimental absorption rate for a 1500 nm thick c-Si solar cell. It is adapted from recently published research [38]. The right figure indicates the absorption rate obtained by the simulation.

very well with the experimental data. For the textured structure, the simulation predicted a slightly lower absorption than observed in experiment, particularly for wavelengths around 800 nm. This is mainly because different texturing methods are used in the simulation and the experiment.

3. Statistical random surface texturing model

A number of recent studies have focused on approaching the Yablonovitch $4n^2$ limit for light trapping by introducing a randomly textured front surface [39, 40]. However, recent work has also demonstrated that this limit can be exceeded within a certain range of wavelengths by introducing deviations from perfectly random structures [41]. Previous simulations have shown that introducing structures that effectively enhance the group index of the structure beyond the bulk material can be highly effective for improving performance within the critical light-trapping regime [42]. However, previous material models in the time domain did not always accurately represent the experimentally observed dispersion properties, thus limiting the potential role for highly accurate simulation techniques such as finite-difference time domain [27–29]. However, combining innovative light trapping structures with adjustable parameters in the presence of properly modeled dispersion can help accurately pinpoint the best structures to build in experiments. It has been observed that over very short distances, the aspect ratios of features in thin-film structures are limited to a process-dependent degree, which renders the perfectly random texture as somewhat unrealistic [40]. Thus, introducing a degree of short-range correlation can help capture the smoothness (finite aspect ratio) of real structures. Furthermore, adding a measure of periodicity into the system opens up the potential for higher group index modes, associated with slow light and resonant absorption phenomena [41, 42]. If we want to create a structure that captures both the limits on the aspect ratios as well as the degree of nearest-neighbor correlation, we can generally represent it mathematically as having a first term that reproduces the neighbor's height with a correlation factor f that varies from zero to one, as well as a second, random term that preserves the norm of the average height:

$$Z_{n+1} = f * Z_n + \sqrt{1 - f^2} * r_n, \qquad (4)$$

where Z_n is the nth height of the random texturing surface and r_n is an independent sampling from a random distribution of Gaussian variables with a zero mean and unit variance. The correlation factor f is thus able to control the randomness of the textured surface. For example,
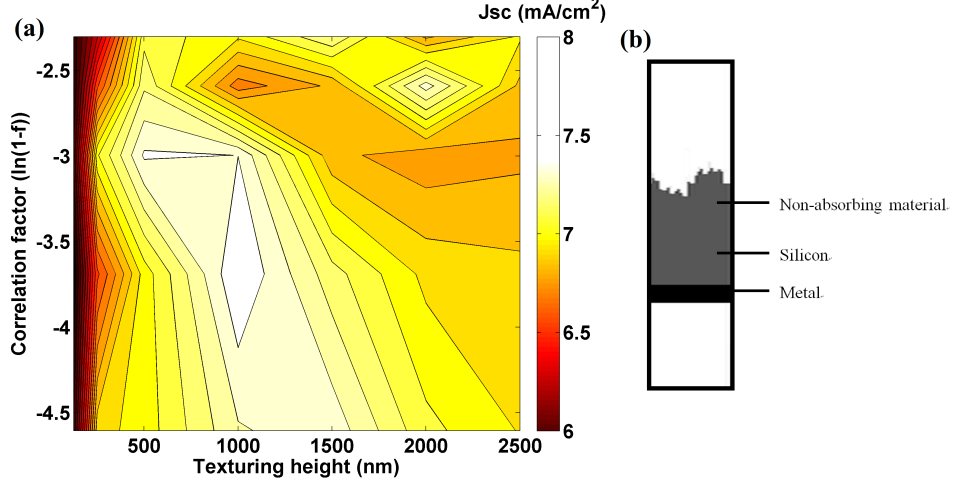
Fig. 5. (a) Contour plot showing calculated short-circuit current density as a function of maximum texturing height and correlation factor for 2D solar cells, using TM-polarized light incident at normal incidence. Note that the optimal performance is expected to occur at $f = 0.975$, $\ln(1 - f) = -3.689$ and $h = 1000$ nm in 2-D structure. (b) The optimized 2D geometry used to generate our contour plot.

when the correlation factor is equal to one, a flat surface is generated; when it reaches zero, Eq. (4) is dominated by r_n, which is a Gaussian variable. However, this formulation does not account for the possibility of periodic boundary conditions. Thus, we extend our definition of correlation from Eq. (4) by introducing a doubly correlated version that accounts for periodicity explicitly:

$$Z_{n+1} = w(n,N) * Z_n + (f - w(n,N)) * Z_{N-n-1} + \sqrt{1 - f^2} * r_n, \tag{5}$$

where N is the maximum index of the 1-D structure and $w()$ denotes a 1-D weighting function:

$$w(n,N) = f - (f/2) * \exp(-(N - 2 * n + 2)), \tag{6}$$

where n ranges from 0 to $N/2$. Note that the textured blocks are created in the following order: $Z_0, Z_N, Z_1, Z_{N-1} \ldots Z_{2/N-1}, Z_{2/N}$. The application of the double-sided correlation function ensures that the textured surface will not have abrupt changes in height at its edges, which could result in an unrealistic randomly textured surface. Note that in general, the exponential decay can have a prefactor Γ in its exponent, but it was set to unity in our work, since we found dependence on this parameter to be fairly weak in our simulations.

A 2-D simulation of the solar cell is performed using a FDTD tool known as MEEP [33] to obtain the optimum texturing height and correlation factor. The algorithm for generating the random surface texturing is based on the double correlation equation above, Eq. (5). In this 2-D simulation, a TM-polarized wave is incident from the normal direction. The structure defined in the 2-D simulation, as shown in Fig. 5, consists of a metal back reflector, a silicon (absorbing material) block with a fixed thickness, and a non-absorbing random surface texturing. The transmission spectrum $T(\lambda)$ and the reflection spectrum $R(\lambda)$ are computed and used to compute the absorption spectra, $A(\lambda) = 1 - T(\lambda) - R(\lambda)$ over a specified range of wavelengths. The absorption is then fed into the short-circuit current density (J_{sc}) which serves as a proxy for the efficiency of the photovoltaic cells.
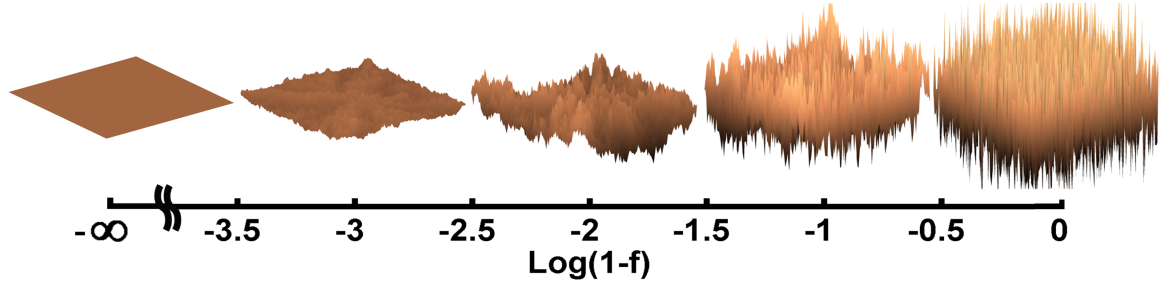
Fig. 6. Random surface texturing algorithm represented in terms of correlation factor (f).

As depicted in Fig. 5, the highest J_{sc} of 7.466 mA/cm^2 is obtained at the optimum texturing height of 1000 nm and the correlation factor of 0.975. Each J_{sc} value is collected from multiple simulations of runs (5 runs) and averaged out for plotting the contour plot. This provides a proof of concept that correlated random structures can provide additional light absorption.

In order to consider a more realistic 3-D solar cell structure, the 1-D double-sided correlation equation is now expanded over a 2-D surface. Much like the previous extension of the 1-D correlation equation to account for periodic boundary conditions in Eq. (5), the 2-D double-sided correlation equation extends this in both periodic directions as follows:

$$
\begin{aligned}
Z_{i+1,j+1} = \; & w(i,N_i) * Z_{i,j+1} \\
& + (f/2 - w(i,N_i)) * Z_{N+2-i,j+1} \\
& + w(j,N_j) * Z_{i+1,j} \\
& + (f/2 - w(j,N_j)) * Z_{i+1,N+2-j} \\
& + \sqrt{1-f^2} * r_n,
\end{aligned}
\tag{7}
$$

where i represents the x index, j represents the y index, N_i is the maximum index of i, N_j is the maximum index of j and $w()$ denotes a 2-D weighting function:

$$
\begin{aligned}
w(i,N_i) &= f/2 - (f/4) * \exp(-(N_i - 2*i + 2)), \\
w(j,N_j) &= f/2 - (f/4) * \exp(-(N_j - 2*j + 2)).
\end{aligned}
\tag{8}
$$

The textured features of the 2-D surface are created in a similar fashion to those in the original 1-D texturing algorithm. As depicted in Fig. 6, Eq. (7) introduces correlations across the 2-D surface, which reflects the limited aspect ratios associated with random texturing methods. The maximum texturing height of the random surfaces is controlled simply by rescaling the standard deviation (σ) of the Gaussian distribution. The application of long-range periodicity enhances diffraction into guided modes and saves a tremendous amount of computational cost, since simulating a single segment of a periodic structure can closely approximate the entire architecture of a large 3-D solar cell.

Due to the differing resolutions employed in our 2-D and 3-D solar cell simulations, the optimum correlation factor obtained in each simulation also differs. In order to compare them properly, the correlation factor from the 3-D simulation result is exponentiated by a factor given by the product of the block width N times the ratio of the y-grid values in absolute units (e.g., in nm) as shown in the equation below:
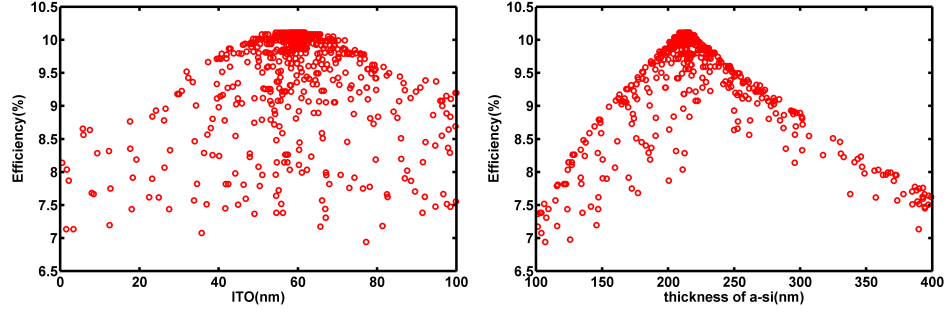
Fig. 7. Efficiency versus thickness of (left) indium-tin oxide and (right) a-Si thickness. Each red dot corresponds to a single 3-D FDTD simulation and is projected from a higher-dimension manifold of design space onto the axes displayed, in order to identify the optimal values for these individual parameters. Note that each simulation is performed in a flat solar cell structure without texturing.

$$f_{2D} = f_{3D}^{(N\Delta y2D/\Delta y3D)}, \tag{9}$$

where $\Delta y2D$ and $\Delta y3D$ are the grid values used in the 2-D and 3-D simulations, respectively. Given that the optimum correlation factor for 2-D simulation is 0.975, its normalized 3-D correlation factor is equal to 0.9998.

It can be useful to compare these results with recent experimental work on thin-film textures for light-trapping. The specific random texturing methods discussed in a recent comprehensive study [40] gave rise to several local peaks, with widths of approximately 50 — 100 nm. Comparing the local peak width of the experimental geometry with our random surface texturing statistical model, the sample with $f = 0.99$ matches well with the structure introduced in the reference paper [40]. Looking at the surfaces shown in Fig. 6, one hardly can distinguish which one will be the best light trapping structure among a variety of randomly-textured surfaces. It will become more apparent when these randomly-textured surfaces are applied to the front of the solar cell structure.

4. Enhanced light trapping in a tandem cell application

In this section, we numerically demonstrate the optimum front texturing of a silicon tandem solar cell by utilizing the approach outlined in the previous sections to create a correlated random texturing and to accurately simulate its behavior in the time domain. The QCRF-FDTD and the statistical random texturing models are used both to enhance light trapping in a tandem cell structure and to help match the current generation in each layer.

The efficiency as a function of the thicknesses of a-Si:H, c-Si:H and ITO layers in a flat tandem cell structure is shown in Fig. 7. In order to find the best thicknesses, we first run 3-D FDTD simulations after varying all the geometric parameters. We then project these results onto a single axis at a time, while look for a cluster of points with the highest calculated efficiencies. Using this procedure, we find that the optimum thicknesses of a-Si:H and c-Si:H are 205 nm and 1795 nm, respectively; ITO had its best performance when its thickness is 60 nm.

Starting with the best parameters observed in Fig. 7, the statistical texturing algorithm is applied to determine the optimum surface texturing of the tandem cell structure. As shown in Fig. 1, the same randomly textured surface is applied to the ITO, a-Si and c-Si layers. Because
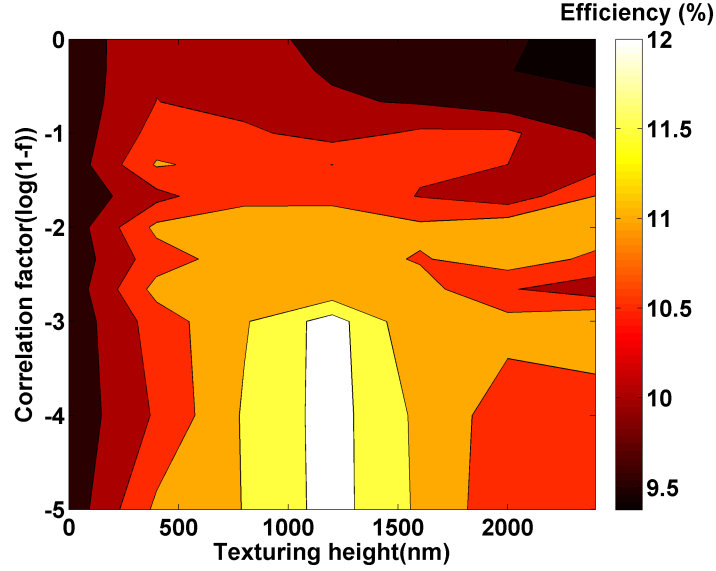
Fig. 8. Contour plot showing silicon tandem cell efficiency versus texturing height and the correlation factor. Note that the optimal performance is predicted to occur when $f = 0.999$ and $h = 1158$ nm, as explained in the text.

a maximum texturing height is also considered as an important factor in random texturing, we introduce a feature which controls the maximum texturing height of the random texturing algorithm. In order to calculate the overall cell efficiency of the cell, the internal quantum efficiency of a-Si and c-Si are calculated from a semiclassical drift-diffusion simulation tool capable of calculating recombination losses known as ADEPT 2.0 [43]. In the combination of recombination and optical losses, the overall cell efficiencies of the random texturing model are plotted as shown in Fig. 8. The best cell efficiency is 12.37%; the associated short circuit currents are 12.79 mA/cm^2 at the a-Si layer and 12.88 mA/cm^2, while the open circuit voltages are 875.9 mV for the a-Si layer and 520.0 mV for the c-Si layer. The optimum texturing height is 1158 nm and the optimum correlation factor is 0.999. The efficiency of cell tends to plateau after it reaches a high enough correlation factor of 0.999 or more. The reason is that our algorithm re-scales the height of random structures in order to find the optimum texturing height, so that random surfaces with higher correlation factors tend to create structures very similar to those obtained with lower correlation factors. Thus we can feel confident that we have found a global optimum with respect to these two key parameter values.

Light absorption of the a-Si and c-Si layers is shown in Fig. 9. We compare the best-performing structure from Fig. 8 with flat ($f = 1$) and totally random ($f = 0$) structures at normal incidence. In the a-Si layer, the optimized structure shows enhanced light trapping over the entire range of wavelengths. The absorption of c-Si shown in Fig. 9 (b) should not be directly compared to each structure, because the amount of light arriving at the c-Si layer is different due to a filtering effect caused by absorption in the a-Si layer. Thus, light absorption in the c-Si layer is re-normalized by including that effect. Fig. 9 (c) shows that the normalized absorption in the c-Si layer is also enhanced, compared to both the flat and random structures. Excepting the Fresnel reflection associated with the air-SiO$_2$ boundary (0.0349 from analytical calculation), the optimized tandem cell has almost full absorption for wavelengths from 300 nm to 550 nm; after that, it decreases as shown in Fig. 9 (d). Front texturing itself with the statistical algorithm shows promising light absorption enhancement for normal incidence; however, it
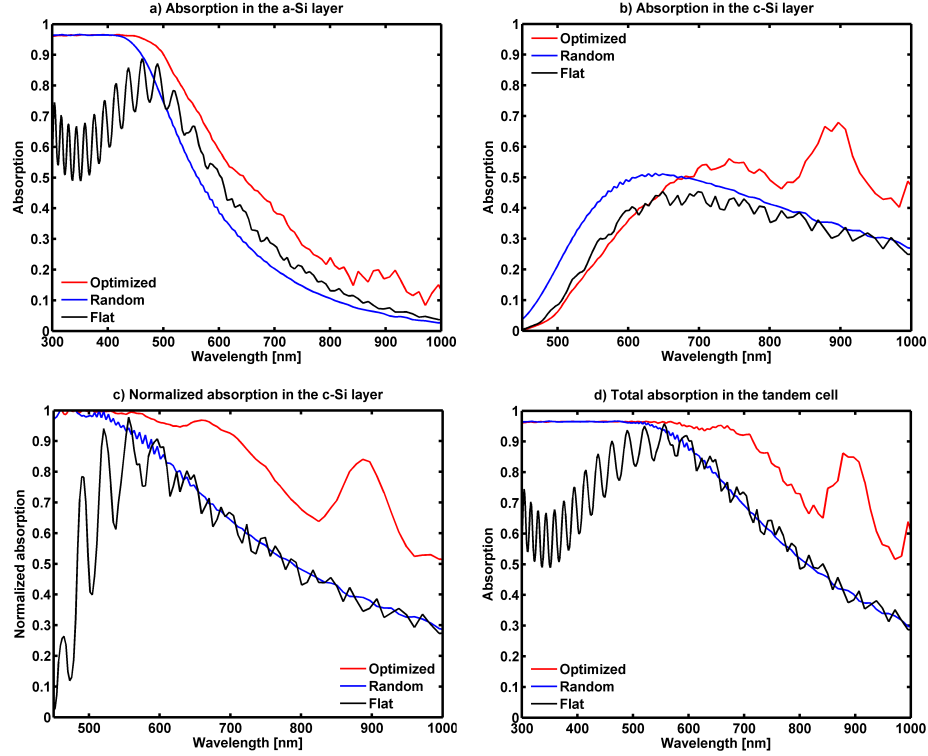
Fig. 9. Light absorption rate of the optimized tandem silicon solar cell with two reference absorption curves that are obtained from a flat structure and a totally random structure for normal incidence. (a) Light absorption in the a-Si layer. (b) Light absorption in the a-Si layer. (c) Normalized light absorption in the c-Si layer with rest of light filtered by the a-Si layer and by subtraction of the first reflected light at the SiO_2 layer. (d) Total light absorption in both layers.

would not be expected to retain the same advantage at all angles. In future work, this shortcoming should be addressed and studied over all angles by adding complementary light trapping methods, such as photonic crystal [44, 45], back grating [46, 47] and intermediate layers [48].

The random textured surface of the best-performing cell is shown in Fig. 10. It has a large structure close to the x-axis, which is connected to the opposite side via periodic boundary conditions, and also has a number of small random structures on its surface. It seems like that a combination of one large structure and several small structures ensures that incident light will be scattered in all directions, so that enhanced absorption can be achieved. It is shown that an enhanced light trapping structure can be obtained by adjusting the correlation factor and the texturing height in our random texturing algorithm.

Also, it should be emphasized that each simulation in Fig. 8 takes approximately 75 hours on a single core computer; entire ensembles of simulations are performed on our computational cluster, Conte, on a dedicated queue that has 64 cores with a memory capacity of 4GB/core. Without an accurate dispersion model, simulating the full bandwidth at an acceptable frequency resolution (as shown in Fig. 9) would not be viable with such a computational resource. In this work, the QCRF dispersion model enables us to reduce a potentially large number of simulations to a *single* calculation over the *entire* relevant portion of the solar spectrum for a given geometry.
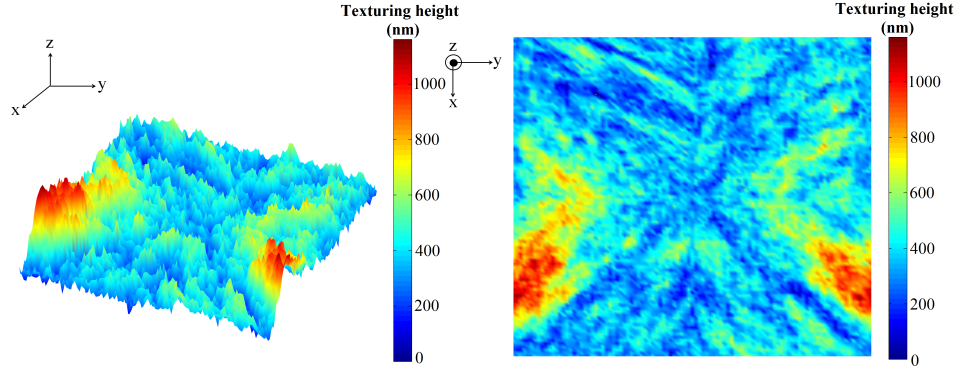
Fig. 10. Optimal random surface texturing in a tandem cell application shown from two different perspectives.

5.   Conclusion

In conclusion, we have investigated a randomly textured surface in a-Si/c-Si micromorph tandem cells using correlated random texturing with QCRF to calculate the entire solar spectrum in a single calculation. The QCRF model satisfies the Kramers-Kronig relation for real materials, is numerically stable, and can be used to achieve accurate curve fitting to experimental semiconductor material dispersion data (e.g., a-Si, c-Si and silver) for wavelengths ranging from 300—1000 nm. Its accuracy is verified in two ways: first, by comparing the results it produced with experimental results acquired for photovoltaic materials; and second, in comparing this simulation technique with analytical results, where the root mean squared error is observed to be 3.967%. The QCRF model is applied to a 3-D FDTD simulation; used properly, it reduces a potentially large number of simulations required for full solar spectrum analysis to a *single* simulation run. Taking advantage of this capability, a range of correlated random textures for light trapping are examined to find the optimal parameter values. Constraining ourselves to a 2 μm-thick active material combination of a-Si/c-Si, we have found that the best-performing micromorph tandem cell structure has 1158 nm of maximum texturing height and a relatively high correlation factor ($f = 0.999$). It is predicted to have 12.37% stabilized cell efficiency, 12.79 mA/cm^2 of short-circuit current and 1395.9 mV of open-circuit voltage. In short, a randomly textured tandem cell with optimized parameters shows meaningful enhancement of light absorption at normal incidence. In future work, alternative and complementary designs with more general applicability will be considered, including but not limited to photonic crystal structures [44,45], back grating [46,47] and intermediate layer [48]. In all these cases, as well as for other photovoltaic absorber or window layer materials, the QCRF and statistical texturing models can play a critical role in enabling accurate single simulations encompassing the entire solar spectrum.